universe

IMPACT FACTOR 2.5

CITESCORE 4.3

Communication

Constraints on the Primordial Curvature Power Spectrum and Reheating Temperature from the NANOGrav 15-Year Dataset

Qin Fei

MDPI

https://doi.org/10.3390/universe10060251 *universe*

MDPI

Communication

Constraints on the Primordial Curvature Power Spectrum and Reheating Temperature from the NANOGrav 15-Year Dataset

Qin Fei

School of Mathematics and Physics, Hubei Polytechnic University, Huangshi 435003, China; feiqin@hbpu.edu.cn

Abstract: The stochastic signal observed by collaborations such as NANOGrav, PPTA, EPTA +InPTA, and CPTA may originate from gravitational waves induced by primordial curvature perturbations during inflation. This study investigates small-scale properties of inflation and reheating, assuming a log-normal form for the power spectrum of the primordial curvature and a reheating phase equation of state $w = 1/9$. Inflation and reheating scenarios are thoroughly examined using Bayesian methods applied to the NANOGrav 15-year dataset. The analysis establishes constraints on the reheating temperature, suggesting $T_{\rm rh} \gtrsim 0.1$ Gev, consistent with Big Bang nucleosynthesis constraints. Additionally, the NANOGrav 15-year dataset requires the amplitude ($A \sim 0.1$) and width ($\Delta \lesssim 0.001$) of the primordial curvature power spectrum to be within specific ranges. A notable turning point in the energy density of scalar-induced gravitational waves occurs due to a change in the equation of state w. This turning point signifies a transition from the reheating epoch to radiation domination. Further observations of scalar-induced gravitational waves could provide insights into the precise timing of this transition, enhancing our understanding of early Universe dynamics.

Keywords: PTA; inflation; reheating

1. Introduction

The detection of gravitational waves (GWs) resulting from compact binary mergers by the LIGO–Virgo–KAGRA collaboration [1–3] represents a groundbreaking achievement in astrophysics and cosmology, significantly advancing our understanding of the diverse population of GW sources [4–15]. This milestone has opened avenues for exploring stochastic GW backgrounds, which promise profound insights into various astrophysical and cosmological phenomena [16,17], such as dark matter [18–20] and modified gravity [21–26].

Recent observations from multiple pulsar timing array (PTA) collaborations—including at the North American Nanohertz Observatory for Gravitational Waves (NANOGrav) [27,28], Parkes Pulsar Timing Array (PPTA) [29,30], European Pulsar Timing Array (EPTA) in combination with Indian Pulsar Timing Array (InPTA) [31,32], and Chinese Pulsar Timing Array (CPTA) [33]—have revealed a common spectrum signal characterized by the Hellings–Downs angular correlation feature inherent in GWs. This distinctive signal, resembling a fiducial characteristic strain spectrum of $f^{-2/3}$, is regarded as an ensemble of inspiraling supermassive black hole binaries by default [27,30,32,33]. However, alternative interpretations are also possible, and uncovering the precise origin of this interesting signal remains an active area of investigation [34–69]. For more about the physical processes generating GWs with the PTA band, see [70–80].

Scalar-induced gravitational waves (SIGWs), linked to the formation of primordial black holes (PBHs), originate from secondary orders of linear scalar perturbations during the inflationary epoch, and these perturbations are seeded by primordial curvature perturbations, as extensively discussed in the literature [5,7,9,11–13,81–124]. Generating significant SIGWs requires amplifying the amplitude of the primordial curvature power spectrum. This amplification is often realized by inflationary models that incorporate transitional ultra-slow-roll phases [91,125–166]. The frequencies of the peak of SIGWs are

check for updates

Citation: Fei, Q. Constraints on the Primordial Curvature Power Spectrum and Reheating Temperature from the NANOGrav 15-Year Dataset. *Universe* **2024**, *10*, 251. https://doi.org/10.3390/universe10060251

Academic Editor: Øyvind Grøn

Received: 30 April 2024
Revised: 30 May 2024
Accepted: 31 May 2024
Published: 4 June 2024

Copyright: © 2024 by the author. Licensee MDPI, Basel, Switzerland. This article is an open access article distributed under the terms and conditions of the Creative Commons Attribution (CC BY) license (https://creativecommons.org/licenses/by/4.0/).

intricately linked to the scales of the peak in the power spectrum of primordial curvature perturbations. Specifically, the frequencies of SIGWs in nanohertz (nHz) correspond to the scales characterized by wave numbers on the order of $k_p \sim 10^7$ Mpc^{-1} in the power spectrum of primordial curvature perturbations. This relationship between frequency and scale is critical for understanding the detectability and observational implications of SIGWs in the universe's early history.

This study is centered around analyzing the PTA signal associated with SIGWs, specifically during the reheating epoch, with the equation of state being $w = 1/9$ before the radiation-dominated era. This particular equation of state emerges within the framework of a scalar field and offers a solution to the problem of excessive PBH production observed when fitting PTA data with SIGWs. Recent investigations have underscored challenges linked to this issue, highlighting the significance of non-Gaussianity in primordial curvature perturbations [38,39,167]. Our study aims to rigorously constrain inflationary and reheating scenarios by employing Bayesian methods applied to the NANOGrav 15-year dataset within the context of the equation of state $w = 1/9$.

To organize our analysis effectively, we structure our discussion as follows: Section 2 offers a succinct review of the energy density of SIGWs. Section 3 presents our findings and interpretations derived from the analysis. Finally, Section 4 concludes our study, summarizing key insights and implications. Throughout this work, we adopt natural units, where the speed of light $c = 1$.

2. Scalar-Induced Gravitational Waves

In this section, we delve into a cosmological scenario featuring a reheating epoch with the equation of state parameter satisfying $w = 1/9$, which precedes the onset of Big Bang nucleosynthesis (BBN). Specifically, we focus on a scenario where the transition from the reheating era with $w = 1/9$ to the standard radiation-dominated (RD) era is instantaneous, with the temperature of the Universe at this transition denoted by $T_{\rm rh}$. The $w = 1/9$ reheating scenario was chosen for this study because it represents a non-standard equation of state that can arise in certain inflationary models with non-canonical kinetic terms or non-trivial interactions [168,169]. Investigating this scenario allows us to explore the potential observable consequences of alternative reheating dynamics and broaden our understanding of the range of possible post-inflationary behaviors. Previous investigations of SIGWs in similar scenarios have been conducted [170], where the authors fixed the reheating temperature $T_{\rm rh}$ and the width of the primordial curvature power spectrum. In contrast, our study loosens the constraints on the reheating temperature $T_{\rm rh}$ and the width of the peak in the power spectrum of primordial curvature perturbations. Utilizing Bayesian methods and data from the NANOGrav 15-year dataset, we rigorously constrain both the primordial curvature power spectrum and $T_{\rm rh}$. This method enables us to examine a wider range of parameter space, providing insights into the implications for cosmological models that incorporate SIGWs within these scenarios.

For a general constant equation of state w and constant sound speed c_s, the energy density in a SIGW can be expressed as [86]

$$\Omega_{\rm GW,rh} = \left(\frac{k}{k_{\rm rh}}\right)^{-2b} \int_0^\infty dvs. \int_{|1-v|}^{1+v} du\, \mathcal{T}(u,v,b,c_s)\, \mathcal{P}_{\mathcal{R}}(ku)\, \mathcal{P}_{\mathcal{R}}(kv), \tag{1}$$

where the subscript "rh" denotes the "reheating", $b \equiv (1-3w)/(1+3w)$, and $\mathcal{P}_{\mathcal{R}}$ is the power spectrum of the primordial curvature perturbations. Here, $u = |\mathbf{k} - \tilde{\mathbf{k}}|/k$ and $v = \tilde{k}/k$ are dimensionless variables, where the auxiliary wave number $\tilde{\mathbf{k}}$ comes from the Fourier transform of the second-order source, $k = |\mathbf{k}|$ and $\tilde{k} = |\tilde{\mathbf{k}}|$ [84]. The transfer function $\mathcal{T}(u,v,b,c_s)$ is

$$\begin{aligned}\mathcal{T}(u,v,b,c_s) = \; & \mathcal{N}(b,c_s)\left(\tfrac{4v^2-(1-u^2+v^2)^2}{4u^2v^2}\right)^2|1-y^2|^b \\ & \times\left\{\left(\mathsf{P}_b^{-b}(y)+\tfrac{b+2}{b+1}\mathsf{P}_{b+2}^{-b}(y)\right)^2\Theta(c_s(u+v)-1)\right. \\ & +\tfrac{4}{\pi^2}\left(\mathsf{Q}_b^{-b}(y)+\tfrac{b+2}{b+1}\mathsf{Q}_{b+2}^{-b}(y)\right)^2\Theta(c_s(u+v)-1) \\ & \left.+\tfrac{4}{\pi^2}\left(\mathcal{Q}_b^{-b}(-y)+2\tfrac{b+2}{b+1}\mathcal{Q}_{b+2}^{-b}(-y)\right)^2\Theta(1-c_s(u+v))\right\}.\end{aligned} \tag{2}$$

Here, the variable $y \equiv 1-[1-c_s^2(u-v)^2]/(2c_s^2uv)$, the function $\Theta(x)$ is the Heaviside theta function, and the function $\mathcal{N}(b,c_s)$ is

$$\mathcal{N}(b,c_s) \equiv \frac{4^{2b}}{3c_s^4}\Gamma(b+\tfrac{3}{2})^4\left(\frac{b+2}{2b+3}\right)^2(1+b)^{-2(1+b)}, \tag{3}$$

where the function $\Gamma(x)$ is the Gamma function.

The Ferrers functions $\mathsf{P}_\nu^\mu(x)$ and $\mathsf{Q}_\nu^\mu(x)$, along with Olver's function $\mathcal{Q}_\nu^\mu(x)$ in the transfer function (2), can be expressed using hypergeometric functions. Specifically, they are defined as follows:

$$\mathsf{P}_\nu^\mu(x) = \left(\frac{1+x}{1-x}\right)^{\mu/2}\mathbf{F}(\nu+1,-\nu;1-\mu;\tfrac{1}{2}-\tfrac{1}{2}x), \tag{4}$$

$$\begin{aligned}\mathsf{Q}_\nu^\mu(x) = & \frac{\pi}{2\sin(\mu\pi)}\left(\cos(\mu\pi)\left(\frac{1+x}{1-x}\right)^{\mu/2}\mathbf{F}(\nu+1,-\nu;1-\mu;\tfrac{1}{2}-\tfrac{1}{2}x)\right. \\ & \left.-\frac{\Gamma(\nu+\mu+1)}{\Gamma(\nu-\mu+1)}\left(\frac{1-x}{1+x}\right)^{\mu/2}\mathbf{F}(\nu+1,-\nu;1+\mu;\tfrac{1}{2}-\tfrac{1}{2}x)\right),\end{aligned} \tag{5}$$

$$\begin{aligned}\mathcal{Q}_\nu^\mu(x) = & \frac{\pi}{2\sin(\mu\pi)\Gamma(\nu+\mu+1)}\left(\left(\frac{x+1}{x-1}\right)^{\mu/2}\mathbf{F}(\nu+1,-\nu;1-\mu;\tfrac{1}{2}-\tfrac{1}{2}x)\right. \\ & \left.-\frac{\Gamma(\nu+\mu+1)}{\Gamma(\nu-\mu+1)}\left(\frac{x-1}{x+1}\right)^{\mu/2}\mathbf{F}(\nu+1,-\nu;1+\mu;\tfrac{1}{2}-\tfrac{1}{2}x)\right).\end{aligned} \tag{6}$$

and

$$\mathbf{F}(a,b;c;x) = \frac{1}{\Gamma(c)}F(a,b;c;x), \tag{7}$$

where $F(a,b;c;x)$ is Gauss's hypergeometric function. By utilizing the correspondence between the evolution of the GW's energy density and that of radiation, we can calculate the energy density in the present-day GW. This calculation is

$$\Omega_{\mathrm{GW},0}h^2 \approx 1.62\times10^{-5}\left(\frac{\Omega_{r,0}h^2}{4.18\times10^{-5}}\right)\left(\frac{g_{*r}(T_{\mathrm{rh}})}{106.75}\right)\left(\frac{g_{*s}(T_{\mathrm{rh}})}{106.75}\right)^{-\frac{4}{3}}\Omega_{\mathrm{GW,rh}}, \tag{8}$$

where g_{*r} and g_{*s} are the effective energy and entropy degrees of freedom at the generation of the SIGWs and $\Omega_{r,0}h^2$ is the energy density parameter of the present-day radiation, respectively.

In this study, we adopt the log-normal form for the power spectrum of primordial curvature perturbations, represented as:

$$\mathcal{P}_{\mathcal{R}}(k) = \frac{A}{\sqrt{2\pi}\Delta}\exp\left(-\frac{\ln^2(k/k_*)}{2\Delta^2}\right), \tag{9}$$

where Δ controls the width of the spectrum, k_* determines the peak position in the spectrum, and A denotes the amplitude of the spectrum. This paper focuses on narrow peak spectra with $\Delta \leq 0.1$, a condition supported by our results presented below. For an extremely narrow peak spectrum with $\Delta \to 0$, the log-normal form power spectrum (9) reduces to a δ-function form, $\mathcal{P}_{\mathcal{R}} = Ak_*\delta(k - k_*)$. For a log-normal spectrum with a finite width, the corresponding energy density parameter $\Omega^{(\Delta)}_{\mathrm{GW},0}h^2$ for SIGWs is given by [100]

$$\Omega^{(\Delta)}_{\mathrm{GW},0}h^2 = \mathrm{Erf}\left[\frac{1}{\Delta}\sinh^{-1}\frac{k}{2k_*}\right]\Omega^{(\delta)}_{\mathrm{GW},0}h^2. \tag{10}$$

Here, $\Omega^{(\Delta)}_{\mathrm{GW},0}h^2$ denotes the present energy density in SIGWs from the primordial curvature power spectrum with a finite-width log-normal form, $\Omega^{(\delta)}_{\mathrm{GW},0}h^2$ is the energy density induced by the δ-function form, and the function $\mathrm{Erf}(x)$ denotes the error function.

At the horizon crossing for a wavenumber k, the temperature T is approximately related by:

$$k \simeq \frac{1.5\times10^7}{\mathrm{Mpc}}\left(\frac{g_{*r}(T)}{106.75}\right)^{\frac{1}{2}}\left(\frac{g_{*s}(T)}{106.75}\right)^{-\frac{1}{3}}\left(\frac{T}{\mathrm{GeV}}\right). \tag{11}$$

The corresponding frequency f related to the scale k is:

$$f = \frac{k}{2\pi} \simeq 1.6\,\mathrm{nHz}\left(\frac{k}{10^6\,\mathrm{Mpc}^{-1}}\right). \tag{12}$$

Combining Equations (11) and (12), we establish the relationship between the frequency f and the temperature T as:

$$f \simeq 24\,\mathrm{nHz}\left(\frac{g_{*r}(T)}{106.75}\right)^{\frac{1}{2}}\left(\frac{g_{*s}(T)}{106.75}\right)^{-\frac{1}{3}}\left(\frac{T}{\mathrm{GeV}}\right). \tag{13}$$

It is important to note that there is a minimum requirement for the reheating temperature during BBN, which is $T_{\mathrm{rh}} \geq 4$ MeV, as indicated by various studies [171–174]. Consequently, this imposes an upper limit on the reheating frequency f_{rh}, ensuring that $f_{\mathrm{rh}} \leq 0.1$ nHz, which falls below the sensitivity range of pulsar timing arrays.

3. Methodology and Results

In this section, we proceed under the assumption that the signal in the NANOGrav 15-year dataset originates from gravitational waves induced by the finite-width log-normal form of the primordial curvature power spectrum given in Equation (9). We utilize Bayesian methods on the NANOGrav 15-year dataset to derive constraints on both the primordial curvature power spectrum and the reheating temperature T_{rh}. The analysis involves leveraging the information from the 14 frequency bins in the NANOGrav 15-year dataset [27,34] to infer the posterior distribution of T_{rh} and the parameters within the primordial curvature power spectrum parameterized as Equation (9). We employ the `Bilby` code [175], which implements the `dynesty` algorithm for nested sampling [176], to compute the posterior distribution. To establish the log-likelihood function, we begin by calculating the energy density of scalar-induced gravitational waves at frequencies corresponding to the 14 bins in our analysis. Subsequently, we create the logarithm of the probability density functions using 14 independent kernel density estimates. Finally, we multiply the probabilities from these 14 bins to construct the comprehensive likelihood function [39,43,46,47,177,178]. This formulation is expressed as

$$\mathcal{L}(\Lambda) = \prod_{i=1}^{14}\mathcal{L}_i(\Omega_{\mathrm{GW}}(f_i,\Lambda)). \tag{14}$$

Here, $\Lambda = \{A, \Delta, f_*, T_{\rm rh}\}$ encompasses all the model parameters, covering both those associated with the primordial curvature power spectrum (9) and the reheating temperature $T_{\rm rh}$. The priors for these parameters are specified in Table 1, where $\mathcal{U}$ indicates a uniform distribution.

Figure 1 presents the posterior distributions for the parameters linked to the primordial curvature power spectrum defined in Equation (9), including the reheating temperature denoted as $T_{\rm rh}$. Table 1 compiles the median posterior values and the boundaries of the 90% credible intervals for these parameters. Within the posterior distributions, the relationship between the scale k_* and the corresponding frequency f_* is governed by Equation (12). At a confidence level of 90%, the NANOGrav 15-year dataset requires the width of the power spectrum of primordial curvature to be $\Delta \leq 0.001$, which supports the narrow peak assumption made in Section 2. Moreover, the lower bound on the reheating temperature, $T_{\rm rh} \geq 0.1$ Gev, conforms to the constraints imposed by BBN. The constraints on the amplitude A and the peak scale frequencies f_* of the primordial curvature power spectrum are consistent with those reported in a publication by the NANOGrav Collaboration investigating new physical phenomena [34].

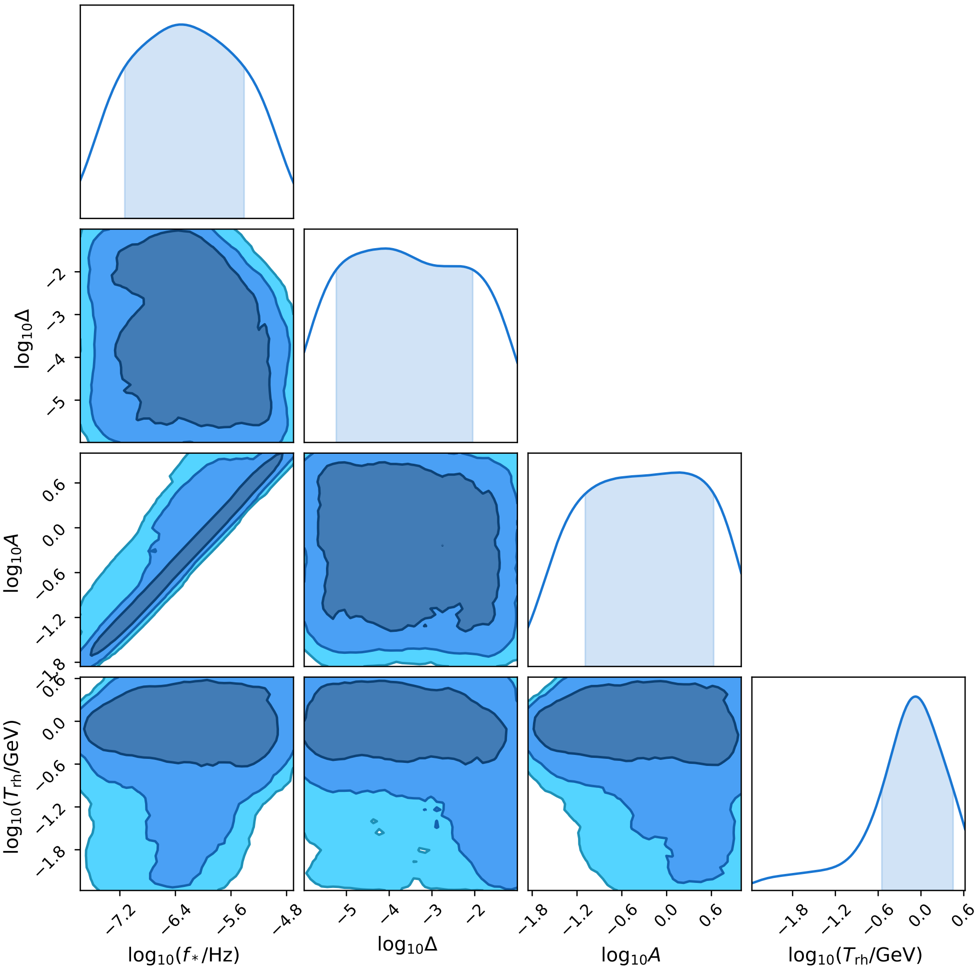

Figure 1. This figure presents the posterior probability distributions for the parameters in the primordial curvature power spectrum parameterization, as described in Equation (9), and the reheating temperature. ($T_{\rm rh}$). The diagonal panels show the marginalized one-dimensional posterior distributions for each parameter, while the off-diagonal panels show the two-dimensional joint posterior distributions, revealing the correlations between parameter pairs. The scale k_* and the corresponding frequency f_* are related through the expression given in Equation (12). The posterior distributions summarize the probabilistic constraints on these parameters based on the analysis of the available data.

Table 1. Summary of the prior distributions, median posterior values, and 90% credible interval bounds for the reheating temperature (T_{rh}) and the parameters associated with the primordial curvature power spectrum, as described in Equation (9). The priors are represented by uniform distributions, denoted by $\mathcal{U}$. The median posterior values provide the most probable estimates for each parameter, while the credible interval bounds of 90% indicate the range within which the true parameter values are likely to lie, based on the given data and the assumed model.

Parameter	$\log_{10}(f_*/\mathrm{Hz})$	$\log_{10}\Delta$	$\log_{10} A$	$\log_{10}(T_{\mathrm{rh}}/\mathrm{GeV})$
prior	$\mathcal{U}(-10,-2)$	$\mathcal{U}(-6,-1)$	$\mathcal{U}(-5,1)$	$\mathcal{U}(-10,-7)$
posterior	$-6.26^{+1.20}_{-1.16}$	$-3.6^{+2.3}_{-2.2}$	$-0.28^{+1.16}_{-1.20}$	$-0.12^{+0.64}_{-1.51}$

Using the optimal parameter values obtained from Table 1, we computed the energy density in SIGWs. The resulting energy density is depicted by the blue line in Figure 2, and the blue region denotes the 1-σ confidence intervals. In particular, around a frequency of approximately $f \sim 10^{-8.1}$ Hz, we observe a notable turning point in the energy density of SIGWs. This turning point corresponds to a change in the equation of state w, which affects the evolution of SIGWs and leads to a distinctive feature in the energy density spectrum.

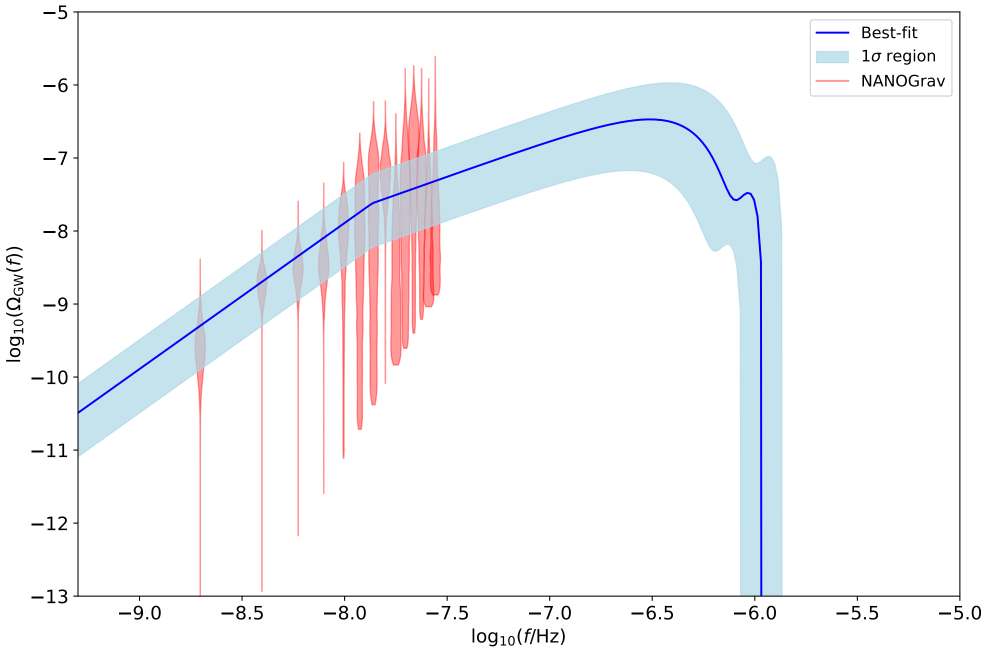

Figure 2. This figure depicts the energy density of the SIGW for parameter values corresponding to the best-fit values. The blue curve in the middle represents the predicted SIGW energy density spectra based on these best-fit parameter sets; the blue region denotes the 1-σ confidence intervals for the energy density of SIGWs. To provide context, the red violin plots illustrate the energy density estimates of the free spectrum obtained from the NANOGrav 15-year dataset. The width of the violins at each frequency indicates the probability density of the energy density. By comparing the predicted SIGW spectra with the NANOGrav observational constraints, this figure allows for an evaluation of the agreement between the best-fit models and the available data.

The energy density spectrum of SIGWs, as shown in Figure 2, exhibits a sharp decrease in the ultraviolet region around the frequency of $f \sim 10^{-6}$. This feature is a characteristic of SIGWs originating from a primordial curvature power spectrum with a narrow peak. In the case of a δ-function form of the primordial curvature power spectrum, $\mathcal{P}_\zeta(k) = A_\zeta \delta[\ln(k/k_*)]$, which represents an extremely narrow peak, the energy density of SIGWs cuts off at scales of $k \geq 2k_*$ [90]. Our data analysis requires a very narrow peak in the primordial curvature power spectrum, with constraints indicating $\Delta < 0.001$. This narrow peak directly results in the observed sharp decrease in the energy density of SIGWs. Therefore, the feature in Figure 2 is a consequence of the primordial curvature power spectrum having a very narrow peak, as necessitated by the PTA data.

4. Conclusions and Discussion

The stochastic signal observed by collaborations such as NANOGrav, PPTA, and EPTA, along with InPTA and CPTA, likely originates from gravitational waves induced by primordial curvature perturbations generated during inflation. Following inflation, the Universe undergoes a reheating phase aimed at increasing its temperature. Information about the small-scale properties of inflation and reheating can be encoded in the energy density of SIGWs. This study explores the small-scale characteristics of inflation and reheating and assumes that the equation of state during the reheating phase is characterized by $w = 1/9$. During the oscillation of the inflaton, $w = \frac{p-2}{p+2}$ for a power-law potential $V(\phi) \propto \phi^p$ [179,180]. The choice $w = 1/9$ corresponds to a scalar field potential of the form $V(\phi) \sim \phi^{5/2}$ near its minimum, which exhibits a flatter minimum compared to the standard quadratic case, leading to distinct reheating dynamics. The $\phi^{5/2}$ potential form can arise in inflationary models with non-canonical kinetic terms, such as k-inflation [181] or DBI inflation [182], or be motivated by considering higher-order corrections to the inflaton potential [183]. The total potential model under consideration includes terms that allow for a smooth transition from the inflationary phase to this specific reheating scenario [184].

To model the power spectrum of the primordial curvature perturbations, a log-normal form is adopted. By applying Bayesian methods and analyzing the NANOGrav 15-year dataset, we obtain posterior distributions for the key parameters. These include the characteristic frequency f_*, the width parameter Δ, the amplitude A of the primordial curvature power spectrum and the reheating temperature $T_{\rm rh}/\mathrm{GeV}$. The obtained posterior values are $\log_{10}(f_*/\mathrm{Hz}) = -6.26^{+1.20}_{-1.16}$, $\log_{10}\Delta = -3.6^{+2.3}_{-2.2}$, $\log_{10} A = -0.28^{+1.16}_{-1.20}$ and $\log_{10}(T_{\rm rh}/\mathrm{GeV}) = -0.12^{+0.64}_{-1.51}$.

It is important to acknowledge that the $w = 1/9$ reheating scenario is one among many possibilities for post-inflationary dynamics. The more commonly assumed scenario is $w = 0$, which corresponds to a quadratic potential minimum [185,186]. However, exploring alternative scenarios, such as $w = 1/9$, allows us to investigate the potential observational signatures of non-standard reheating dynamics and test the robustness of our conclusions. The choice of equation of state during reheating can have significant effects on observable signatures, such as the energy density of scalar-induced gravitational waves [86,101,187]. In the $w = 1/9$ scenario, distinct reheating dynamics can lead to modifications in the spectral shape and amplitude of the gravitational wave background compared to the standard $w = 0$ case. Exploring these alternative scenarios provides valuable insights into the sensitivity of observables to the details of the reheating phase and can help constrain inflationary models based on observational data [188].

Furthermore, the energy density of SIGWs displays a distinctive turning point, which corresponds to a change in the equation of state w. This turning point signifies the transition from the reheating epoch to the radiation-dominated era, highlighting a significant phase in the evolution of the early Universe. Future observational data on scalar-induced gravitational waves hold the potential to refine our understanding further, potentially pinpointing the precise time when the reheating phase transitioned into the radiation-dominated era. Such insights could shed light on fundamental aspects of cosmological evolution during the early Universe and aid in the refinement of theoretical models of inflation and reheating.

Funding: This research was supported in part by the National Natural Science Foundation of China under Grant No. 12305060 and the Talent-Introduction Program of Hubei Polytechnic University under Grant No. 19xjk25R.

Data Availability Statement: No new data were created.

Conflicts of Interest: The author declares no conflicts of interest.

References

1. Abbott, B.P. et al. [LIGO Scientific Collaboration and Virgo Collaboration]. GWTC-1: A Gravitational-Wave Transient Catalog of Compact Binary Mergers Observed by LIGO and Virgo during the First and Second Observing Runs. *Phys. Rev. X* **2019**, *9*, 031040. [CrossRef]
2. Abbott, R. et al. [LIGO Scientific Collaboration and Virgo Collaboration]. GWTC-2: Compact Binary Coalescences Observed by LIGO and Virgo During the First Half of the Third Observing Run. *Phys. Rev. X* **2021**, *11*, 021053. [CrossRef]
3. Abbott, R. et al. [LIGO Scientific Collaboration, Virgo Collaboration, and KAGRA Collaboration]. GWTC-3: Compact Binary Coalescences Observed by LIGO and Virgo during the Second Part of the Third Observing Run. *Phys. Rev. X* **2023**, *13*, 041039. [CrossRef]
4. Abbott, B.P. et al. [LIGO Scientific Collaboration and the Virgo Collaboration]. Binary Black Hole Population Properties Inferred from the First and Second Observing Runs of Advanced LIGO and Advanced Virgo. *Astrophys. J. Lett.* **2019**, *882*, L24. [CrossRef]
5. Chen, Z.C.; Huang, F.; Huang, Q.G. Stochastic Gravitational-wave Background from Binary Black Holes and Binary Neutron Stars and Implications for LISA. *Astrophys. J.* **2019**, *871*, 97. [CrossRef]
6. Luo, H.M.; Lin, W.; Chen, Z.C.; Huang, Q.G. Extraction of gravitational wave signals with optimized convolutional neural network. *Front. Phys.* **2020**, *15*, 14601. [CrossRef]
7. Chen, Z.C.; Huang, Q.G. Distinguishing Primordial Black Holes from Astrophysical Black Holes by Einstein Telescope and Cosmic Explorer. *JCAP* **2020**, *08*, 039. [CrossRef]
8. Abbott, R. et al. [LIGO Scientific Collaboration and the Virgo Collaboration]. Population Properties of Compact Objects from the Second LIGO-Virgo Gravitational-Wave Transient Catalog. *Astrophys. J. Lett.* **2021**, *913*, L7. [CrossRef]
9. Chen, Z.C.; Yuan, C.; Huang, Q.G. Confronting the primordial black hole scenario with the gravitational-wave events detected by LIGO-Virgo. *Phys. Lett. B* **2022**, *829*, 137040. [CrossRef]
10. Abbott, R. et al. [LIGO Scientific Collaboration, Virgo Collaboration, and KAGRA Collaboration]. Population of Merging Compact Binaries Inferred Using Gravitational Waves through GWTC-3. *Phys. Rev. X* **2023**, *13*, 011048. [CrossRef]
11. Chen, Z.C.; Du, S.S.; Huang, Q.G.; You, Z.Q. Constraints on primordial-black-hole population and cosmic expansion history from GWTC-3. *JCAP* **2023**, *03*, 024. [CrossRef]
12. Liu, L.; You, Z.Q.; Wu, Y.; Chen, Z.C. Constraining the merger history of primordial-black-hole binaries from GWTC-3. *Phys. Rev. D* **2023**, *107*, 063035. [CrossRef]
13. Zheng, L.M.; Li, Z.; Chen, Z.C.; Zhou, H.; Zhu, Z.H. Towards a reliable reconstruction of the power spectrum of primordial curvature perturbation on small scales from GWTC-3. *Phys. Lett. B* **2023**, *838*, 137720. [CrossRef]
14. You, Z.Q.; Chen, Z.C.; Liu, L.; Yi, Z.; Liu, X.J.; Wu, Y.; Gong, Y. Constraints on peculiar velocity distribution of binary black holes using gravitational waves with GWTC-3. *JCAP* **2024**, *05*, 031. [CrossRef]
15. Chen, Z.C.; Liu, L. Constraining the nonstandard propagating gravitational waves in the cosmological background with GWTC-3. *arXiv* **2024**, arXiv:2405.10031.
16. Liu, X.J.; You, Z.Q.; Chen, Z.C.; Du, S.S.; Li, A.; Zhu, X.J. On the Spin Period Distribution of Millisecond Pulsars. *Astrophys. J.* **2024**, *962*, 80. [CrossRef]
17. Du, S.S.; Liu, X.J.; Chen, Z.C.; You, Z.Q.; Zhu, X.J.; Zhu, Z.H. On the initial spin period distribution of neutron stars. *arXiv* **2024**, arXiv:2402.14030 .
18. Wei, H.; Chen, Z.C.; Liu, J. Cosmological Constraints on Variable Warm Dark Matter. *Phys. Lett. B* **2013**, *720*, 271–276. [CrossRef]
19. Wei, H.; Liu, J.; Chen, Z.C.; Yan, X.P. Indistinguishability of Warm Dark Matter, Modified Gravity, and Coupled Cold Dark Matter. *Phys. Rev. D* **2013**, *88*, 043510. [CrossRef]
20. Du, S.S.; Wei, J.J.; You, Z.Q.; Chen, Z.C.; Zhu, Z.H.; Liang, E.W. Model-independent determination of H0 and ΩK, 0 using time-delay galaxy lenses and gamma-ray bursts. *Mon. Not. R. Astron. Soc.* **2023**, *521*, 4963–4975. [CrossRef]
21. Chen, Z.C.; Wu, Y.; Wei, H. Post–Newtonian Approximation of Teleparallel Gravity Coupled with a Scalar Field. *Nucl. Phys. B* **2015**, *894*, 422–438. [CrossRef]
22. Wu, Y.; Chen, Z.C.; Wang, J.; Wei, H. $f(T)$ non-linear massive gravity and the cosmic acceleration. *Commun. Theor. Phys.* **2015**, *63*, 701–708. [CrossRef]
23. Huang, Y.; Gong, Y.; Liang, D.; Yi, Z. Thermodynamics of scalar–tensor theory with non-minimally derivative coupling. *Eur. Phys. J. C* **2015**, *75*, 351. [CrossRef]
24. Zhu, Y.; Gong, Y. PPN parameters in gravitational theory with nonminimally derivative coupling. *Int. J. Mod. Phys. D* **2016**, *26*, 1750005. [CrossRef]
25. Gong, Y.; Papantonopoulos, E.; Yi, Z. Constraints on scalar–tensor theory of gravity by the recent observational results on gravitational waves. *Eur. Phys. J. C* **2018**, *78*, 738. [CrossRef]
26. Fanizza, G.; Franchini, G.; Gasperini, M.; Tedesco, L. Comparing the luminosity distance for gravitational waves and electromagnetic signals in a simple model of quadratic gravity. *Gen. Rel. Grav.* **2020**, *52*, 111. [CrossRef]
27. Agazie, G. et al. [The NANOGrav Collaboration]. The NANOGrav 15 yr Data Set: Evidence for a Gravitational-wave Background. *Astrophys. J. Lett.* **2023**, *951*, L8. [CrossRef]
28. Agazie, G. et al. [The NANOGrav Collaboration]. The NANOGrav 15 yr Data Set: Observations and Timing of 68 Millisecond Pulsars. *Astrophys. J. Lett.* **2023**, *951*, L9. [CrossRef]
29. Zic, A. et al. [The PPTA Collaboration]. The Parkes Pulsar Timing Array third data release. *Publ. Astron. Soc. Austral.* **2023**, *40*, e049. [CrossRef]

30. Reardon, D.J. et al. [The PPTA Collaboration]. Search for an Isotropic Gravitational-wave Background with the Parkes Pulsar Timing Array. *Astrophys. J. Lett.* **2023**, *951*, L6. [CrossRef]
31. Antoniadis, J. et al. [EPTA Collaboration]. The second data release from the European Pulsar Timing Array—I. The dataset and timing analysis. *Astron. Astrophys.* **2023**, *678*, A48. [CrossRef]
32. Antoniadis, J. et al. [EPTA Collaboration and InPTA Collaboration]. The second data release from the European Pulsar Timing Array - III. Search for gravitational wave signals. *Astron. Astrophys.* **2023**, *678*, A50. [CrossRef]
33. Xu, H.; Chen, S.; Guo, Y.; Jiang, J.; Wang, B.; Xu, J.; Xue, Z.; Caballero, R.N.; Yuan, J.; Xu, Y.; et al. Searching for the Nano-Hertz Stochastic Gravitational Wave Background with the Chinese Pulsar Timing Array Data Release I. *Res. Astron. Astrophys.* **2023**, *23*, 075024. [CrossRef]
34. Afzal, A. et al. [The NANOGrav Collaboration]. The NANOGrav 15 yr Data Set: Search for Signals from New Physics. *Astrophys. J. Lett.* **2023**, *951*, L11. [CrossRef]
35. Agazie, G. et al. [The NANOGrav Collaboration]. The NANOGrav 15 yr Data Set: Constraints on Supermassive Black Hole Binaries from the Gravitational-wave Background. *Astrophys. J. Lett.* **2023**, *952*, L37. [CrossRef]
36. Antoniadis, J. et al. [EPTA Collaboration]. The second data release from the European Pulsar Timing Array: IV. Implications for massive black holes, dark matter and the early Universe. *arXiv* **2023**, arXiv:2306.16227.
37. Yi, Z.; Gao, Q.; Gong, Y.; Wang, Y.; Zhang, F. Scalar induced gravitational waves in light of Pulsar Timing Array data. *Sci. China Phys. Mech. Astron.* **2023**, *66*, 120404. [CrossRef]
38. Franciolini, G.; Iovino, A., Jr.; Vaskonen, V.; Veermae, H. Recent Gravitational Wave Observation by Pulsar Timing Arrays and Primordial Black Holes: The Importance of Non–Gaussianities. *Phys. Rev. Lett.* **2023**, *131*, 201401. [CrossRef]
39. Liu, L.; Chen, Z.C.; Huang, Q.G. Implications for the non-Gaussianity of curvature perturbation from pulsar timing arrays. *Phys. Rev. D* **2024**, *109*, L061301. [CrossRef]
40. Vagnozzi, S. Inflationary interpretation of the stochastic gravitational wave background signal detected by pulsar timing array experiments. *JHEAp* **2023**, *39*, 81–98. [CrossRef]
41. Cai, Y.F.; He, X.C.; Ma, X.H.; Yan, S.F.; Yuan, G.W. Limits on scalar-induced gravitational waves from the stochastic background by pulsar timing array observations. *Sci. Bull.* **2023**, *68*, 2929–2935. [CrossRef] [PubMed]
42. Bi, Y.C.; Wu, Y.M.; Chen, Z.C.; Huang, Q.G. Implications for the supermassive black hole binaries from the NANOGrav 15-year data set. *Sci. China Phys. Mech. Astron.* **2023**, *66*, 120402. [CrossRef]
43. Wu, Y.M.; Chen, Z.C.; Huang, Q.G. Cosmological interpretation for the stochastic signal in pulsar timing arrays. *Sci. China Phys. Mech. Astron.* **2024**, *67*, 240412. [CrossRef]
44. Franciolini, G.; Racco, D.; Rompineve, F. Footprints of the QCD Crossover on Cosmological Gravitational Waves at Pulsar Timing Arrays. *Phys. Rev. Lett.* **2024**, *132*, 081001. [CrossRef] [PubMed]
45. You, Z.Q.; Yi, Z.; Wu, Y. Constraints on primordial curvature power spectrum with pulsar timing arrays. *JCAP* **2023**, *11*, 065. [CrossRef]
46. Jin, J.H.; Chen, Z.C.; Yi, Z.; You, Z.Q.; Liu, L.; Wu, Y. Confronting sound speed resonance with pulsar timing arrays. *JCAP* **2023**, *09*, 016. [CrossRef]
47. Liu, L.; Chen, Z.C.; Huang, Q.G. Probing the equation of state of the early Universe with pulsar timing arrays. *JCAP* **2023**, *11*, 071. [CrossRef]
48. An, H.; Su, B.; Tai, H.; Wang, L.T.; Yang, C. Phase transition during inflation and the gravitational wave signal at pulsar timing arrays. *arXiv* **2023**, arXiv:2308.00070.
49. Zhang, Z.; Cai, C.; Su, Y.H.; Wang, S.; Yu, Z.H.; Zhang, H.H. Nano-Hertz gravitational waves from collapsing domain walls associated with freeze-in dark matter in light of pulsar timing array observations. *Phys. Rev. D* **2023**, *108*, 095037. [CrossRef]
50. Das, B.; Jaman, N.; Sami, M. Gravitational wave background from quintessential inflation and NANOGrav data. *Phys. Rev. D* **2023**, *108*, 103510. [CrossRef]
51. Balaji, S.; Domènech, G.; Franciolini, G. Scalar-induced gravitational wave interpretation of PTA data: The role of scalar fluctuation propagation speed. *JCAP* **2023**, *10*, 041. [CrossRef]
52. Du, X.K.; Huang, M.X.; Wang, F.; Zhang, Y.K. Did the nHZ Gravitational Waves Signatures Observed By NANOGrav Indicate Multiple Sector SUSY Breaking? *arXiv* **2023**, arXiv:2307.02938.
53. Oikonomou, V.K. Flat energy spectrum of primordial gravitational waves versus peaks and the NANOGrav 2023 observation. *Phys. Rev. D* **2023**, *108*, 043516. [CrossRef]
54. Yi, Z.; You, Z.Q.; Wu, Y.; Chen, Z.C.; Liu, L. Exploring the NANOGrav Signal and Planet-mass Primordial Black Holes through Higgs Inflation. *arXiv* **2023**, arXiv:2308.14688.
55. Yi, Z.; You, Z.Q.; Wu, Y. Model-independent reconstruction of the primordial curvature power spectrum from PTA data. *JCAP* **2024**, *01*, 066. [CrossRef]
56. Chen, Z.C.; Huang, Q.G.; Liu, C.; Liu, L.; Liu, X.J.; Wu, Y.; Wu, Y.M.; Yi, Z.; You, Z.Q. Prospects for Taiji to detect a gravitational-wave background from cosmic strings. *JCAP* **2024**, *03*, 022. [CrossRef]
57. Wu, Y.M.; Chen, Z.C.; Bi, Y.C.; Huang, Q.G. Constraining the graviton mass with the NANOGrav 15 year data set. *Class. Quant. Grav.* **2024**, *41*, 075002. [CrossRef]
58. Bi, Y.C.; Wu, Y.M.; Chen, Z.C.; Huang, Q.G. Constraints on the velocity of gravitational waves from the NANOGrav 15-year data set. *Phys. Rev. D* **2024**, *109*, L061101. [CrossRef]

59. Chen, Z.C.; Wu, Y.M.; Bi, Y.C.; Huang, Q.G. Search for nontensorial gravitational-wave backgrounds in the NANOGrav 15-year dataset. *Phys. Rev. D* **2024**, *109*, 084045. [CrossRef]
60. Liu, L.; Wu, Y.; Chen, Z.C. Simultaneously probing the sound speed and equation of state of the early Universe with pulsar timing arrays. *JCAP* **2024**, *04*, 011. [CrossRef]
61. Fei, Q. Constraints on the primordial curvature power spectrum by pulsar timing array data: A polynomial parameterization approach. *Commun. Theor. Phys.* **2024**, *76*, 015404. [CrossRef]
62. Chen, Z.C.; Li, S.L.; Wu, P.; Yu, H. NANOGrav hints for first-order confinement-deconfinement phase transition in different QCD-matter scenarios. *Phys. Rev. D* **2024**, *109*, 043022. [CrossRef]
63. Wang, Z.; Lei, L.; Jiao, H.; Feng, L.; Fan, Y.Z. The nanohertz stochastic gravitational wave background from cosmic string loops and the abundant high redshift massive galaxies. *Sci. China Phys. Mech. Astron.* **2023**, *66*, 120403. [CrossRef]
64. Chen, Z.C.; Liu, L. Is PSR J0514−4002E in a PBH-NS binary? *arXiv* **2024**, arXiv:2401.12889.
65. Chen, Z.C.; Liu, L. Can we distinguish the adiabatic fluctuations and isocurvature fluctuations with pulsar timing arrays? *arXiv* **2024**, arXiv:2402.16781.
66. Chen, Z.C.; Li, J.; Liu, L.; Yi, Z. Probing the speed of scalar-induced gravitational waves with pulsar timing arrays. *Phys. Rev. D* **2024**, *109*, L101302. [CrossRef]
67. Chen, Z.C.; Liu, L. Detecting a Gravitational-Wave Background from Null Energy Condition Violation: Prospects for Taiji. *arXiv* **2024**, arXiv:2404.08375.
68. Chen, Z.C.; Liu, L. Constraints on Inflation with Null Energy Condition Violation from Advanced LIGO and Advanced Virgo's First Three Observing Runs. *arXiv* **2024**, arXiv:2404.07075.
69. Geller, M.; Ghosh, S.; Lu, S.; Tsai, Y. Challenges in interpreting the NANOGrav 15-year dataset as early Universe gravitational waves produced by an ALP induced instability. *Phys. Rev. D* **2024**, *109*, 063537. [CrossRef]
70. Zhu, X.J.; Cui, W.; Thrane, E. The minimum and maximum gravitational-wave background from supermassive binary black holes. *Mon. Not. R. Astron. Soc.* **2019**, *482*, 2588–2596. [CrossRef]
71. Li, J.; Chen, Z.C.; Huang, Q.G. Measuring the tilt of primordial gravitational-wave power spectrum from observations. *Sci. China Phys. Mech. Astron.* **2019**, *62*, 110421; Erratum in *Sci. China Phys. Mech. Astron.* **2021**, *64*, 250451. [CrossRef]
72. Chen, Z.C.; Yuan, C.; Huang, Q.G. Non-tensorial gravitational wave background in NANOGrav 12.5-year data set. *Sci. China Phys. Mech. Astron.* **2021**, *64*, 120412. [CrossRef]
73. Wu, Y.M.; Chen, Z.C.; Huang, Q.G. Constraining the Polarization of Gravitational Waves with the Parkes Pulsar Timing Array Second Data Release. *Astrophys. J.* **2022**, *925*, 37. [CrossRef]
74. Chen, Z.C.; Wu, Y.M.; Huang, Q.G. Searching for isotropic stochastic gravitational-wave background in the international pulsar timing array second data release. *Commun. Theor. Phys.* **2022**, *74*, 105402. [CrossRef]
75. Chen, Z.C.; Wu, Y.M.; Huang, Q.G. Search for the Gravitational-wave Background from Cosmic Strings with the Parkes Pulsar Timing Array Second Data Release. *Astrophys. J.* **2022**, *936*, 20. [CrossRef]
76. Wu, Y.M.; Chen, Z.C.; Huang, Q.G.; Zhu, X.; Bhat, N.D.R.; Feng, Y.; Hobbs, G.; Manchester, R.N.; Russell, C.J.; Shannon, R.M. Constraining ultralight vector dark matter with the Parkes Pulsar Timing Array second data release. *Phys. Rev. D* **2022**, *106*, L081101. [CrossRef]
77. Falxa, M. et al. [IPTA Collaboration]. Searching for continuous Gravitational Waves in the second data release of the International Pulsar Timing Array. *Mon. Not. R. Astron. Soc.* **2023**, *521*, 5077–5086. [CrossRef]
78. Wu, Y.M.; Chen, Z.C.; Huang, Q.G. Search for stochastic gravitational-wave background from massive gravity in the NANOGrav 12.5-year dataset. *Phys. Rev. D* **2023**, *107*, 042003. [CrossRef]
79. Wu, Y.M.; Chen, Z.C.; Huang, Q.G. Pulsar timing residual induced by ultralight tensor dark matter. *JCAP* **2023**, *09*, 021. [CrossRef]
80. Agazie, G. et al. [The International Pulsar Timing Array Collaboration]. Comparing Recent Pulsar Timing Array Results on the Nanohertz Stochastic Gravitational-wave Background. *Astrophys. J.* **2024**, *966*, 105. [CrossRef]
81. Hawking, S. Gravitationally collapsed objects of very low mass. *Mon. Not. R. Astron. Soc.* **1971**, *152*, 75. [CrossRef]
82. Carr, B.J.; Hawking, S.W. Black holes in the early Universe. *Mon. Not. R. Astron. Soc.* **1974**, *168*, 399–415. [CrossRef]
83. Ananda, K.N.; Clarkson, C.; Wands, D. The Cosmological gravitational wave background from primordial density perturbations. *Phys. Rev. D* **2007**, *75*, 123518. [CrossRef]
84. Baumann, D.; Steinhardt, P.J.; Takahashi, K.; Ichiki, K. Gravitational Wave Spectrum Induced by Primordial Scalar Perturbations. *Phys. Rev. D* **2007**, *76*, 084019. [CrossRef]
85. Saito, R.; Yokoyama, J. Gravitational wave background as a probe of the primordial black hole abundance. *Phys. Rev. Lett.* **2009**, *102*, 161101. Erratum in *Phys. Rev. Lett.* **2011**, *107*, 069901. [CrossRef] [PubMed]
86. Domènech, G. Scalar Induced Gravitational Waves Review. *Universe* **2021**, *7*, 398. [CrossRef]
87. Alabidi, L.; Kohri, K.; Sasaki, M.; Sendouda, Y. Observable Spectra of Induced Gravitational Waves from Inflation. *JCAP* **2012**, *09*, 017. [CrossRef]
88. Sasaki, M.; Suyama, T.; Tanaka, T.; Yokoyama, S. Primordial black holes—Perspectives in gravitational wave astronomy. *Class. Quant. Grav.* **2018**, *35*, 063001. [CrossRef]
89. Nakama, T.; Silk, J.; Kamionkowski, M. Stochastic gravitational waves associated with the formation of primordial black holes. *Phys. Rev. D* **2017**, *95*, 043511. [CrossRef]

90. Kohri, K.; Terada, T. Semianalytic calculation of gravitational wave spectrum nonlinearly induced from primordial curvature perturbations. *Phys. Rev. D* **2018**, *97*, 123532. [CrossRef]
91. Di, H.; Gong, Y. Primordial black holes and second order gravitational waves from ultra-slow-roll inflation. *JCAP* **2018**, *07*, 007. [CrossRef]
92. Cheng, S.L.; Lee, W.; Ng, K.W. Primordial black holes and associated gravitational waves in axion monodromy inflation. *JCAP* **2018**, *07*, 001. [CrossRef]
93. Lu, Y.; Gong, Y.; Yi, Z.; Zhang, F. Constraints on primordial curvature perturbations from primordial black hole dark matter and secondary gravitational waves. *JCAP* **2019**, *12*, 031. [CrossRef]
94. Cai, R.G.; Pi, S.; Wang, S.J.; Yang, X.Y. Resonant multiple peaks in the induced gravitational waves. *JCAP* **2019**, *05*, 013. [CrossRef]
95. Cai, R.g.; Pi, S.; Sasaki, M. Gravitational Waves Induced by non-Gaussian Scalar Perturbations. *Phys. Rev. Lett.* **2019**, *122*, 201101. [CrossRef] [PubMed]
96. Cai, R.G.; Pi, S.; Wang, S.J.; Yang, X.Y. Pulsar Timing Array Constraints on the Induced Gravitational Waves. *JCAP* **2019**, *10*, 059. [CrossRef]
97. Cai, R.G.; Guo, Z.K.; Liu, J.; Liu, L.; Yang, X.Y. Primordial black holes and gravitational waves from parametric amplification of curvature perturbations. *JCAP* **2020**, *06*, 013. [CrossRef]
98. Wu, Y. Merger history of primordial black-hole binaries. *Phys. Rev. D* **2020**, *101*, 083008. [CrossRef]
99. Cai, R.G.; Ding, Y.C.; Yang, X.Y.; Zhou, Y.F. Constraints on a mixed model of dark matter particles and primordial black holes from the galactic 511 keV line. *JCAP* **2021**, *03*, 057. [CrossRef]
100. Pi, S.; Sasaki, M. Gravitational Waves Induced by Scalar Perturbations with a Lognormal Peak. *JCAP* **2020**, *09*, 037. [CrossRef]
101. Domènech, G.; Pi, S.; Sasaki, M. Induced gravitational waves as a probe of thermal history of the universe. *JCAP* **2020**, *08*, 017. [CrossRef]
102. Liu, L.; Guo, Z.K.; Cai, R.G. Effects of the surrounding primordial black holes on the merger rate of primordial black hole binaries. *Phys. Rev. D* **2019**, *99*, 063523. [CrossRef]
103. Liu, L.; Guo, Z.K.; Cai, R.G. Effects of the merger history on the merger rate density of primordial black hole binaries. *Eur. Phys. J. C* **2019**, *79*, 717. [CrossRef]
104. Liu, L.; Guo, Z.K.; Cai, R.G.; Kim, S.P. Merger rate distribution of primordial black hole binaries with electric charges. *Phys. Rev. D* **2020**, *102*, 043508. [CrossRef]
105. Liu, L.; Yang, X.Y.; Guo, Z.K.; Cai, R.G. Testing primordial black hole and measuring the Hubble constant with multiband gravitational-wave observations. *JCAP* **2023**, *01*, 006. [CrossRef]
106. Chen, Z.C.; Yuan, C.; Huang, Q.G. Pulsar Timing Array Constraints on Primordial Black Holes with NANOGrav 11-Year Dataset. *Phys. Rev. Lett.* **2020**, *124*, 251101. [CrossRef] [PubMed]
107. Yuan, C.; Chen, Z.C.; Huang, Q.G. Scalar induced gravitational waves in different gauges. *Phys. Rev. D* **2020**, *101*, 063018. [CrossRef]
108. Yuan, C.; Chen, Z.C.; Huang, Q.G. Log-dependent slope of scalar induced gravitational waves in the infrared regions. *Phys. Rev. D* **2020**, *101*, 043019. [CrossRef]
109. Yuan, C.; Chen, Z.C.; Huang, Q.G. Probing primordial–black-hole dark matter with scalar induced gravitational waves. *Phys. Rev. D* **2019**, *100*, 081301. [CrossRef]
110. Carr, B.; Kohri, K.; Sendouda, Y.; Yokoyama, J. Constraints on primordial black holes. *Rept. Prog. Phys.* **2021**, *84*, 116902. [CrossRef]
111. Liu, L.; Christiansen, O.; Guo, Z.K.; Cai, R.G.; Kim, S.P. Gravitational and electromagnetic radiation from binary black holes with electric and magnetic charges: Circular orbits on a cone. *Phys. Rev. D* **2020**, *102*, 103520. [CrossRef]
112. Liu, L.; Christiansen, O.; Ruan, W.H.; Guo, Z.K.; Cai, R.G.; Kim, S.P. Gravitational and electromagnetic radiation from binary black holes with electric and magnetic charges: Elliptical orbits on a cone. *Eur. Phys. J. C* **2021**, *81*, 1048. [CrossRef]
113. Yi, Z.; Fei, Q. Constraints on primordial curvature spectrum from primordial black holes and scalar-induced gravitational waves. *Eur. Phys. J. C* **2023**, *83*, 82. [CrossRef]
114. Papanikolaou, T.; Tzerefos, C.; Basilakos, S.; Saridakis, E.N. Scalar induced gravitational waves from primordial black hole Poisson fluctuations in f(R) gravity. *JCAP* **2022**, *10*, 013. [CrossRef]
115. Papanikolaou, T.; Tzerefos, C.; Basilakos, S.; Saridakis, E.N. No constraints for f(T) gravity from gravitational waves induced from primordial black hole fluctuations. *Eur. Phys. J. C* **2023**, *83*, 31. [CrossRef]
116. Chakraborty, A.; Chanda, P.K.; Pandey, K.L.; Das, S. Formation and Abundance of Late-forming Primordial Black Holes as Dark Matter. *Astrophys. J.* **2022**, *932*, 119. [CrossRef]
117. Liu, L.; Kim, S.P. Gravitational and electromagnetic radiations from binary black holes with electric and magnetic charges. *arXiv* **2022**, arXiv:2201.01138.
118. Chen, Z.C.; Huang, Q.G. Merger Rate Distribution of Primordial-Black-Hole Binaries. *Astrophys. J.* **2018**, *864*, 61. [CrossRef]
119. Liu, L.; Kim, S.P. Merger rate of charged black holes from the two-body dynamical capture. *JCAP* **2022**, *03*, 059. [CrossRef]
120. Chen, Z.C.; Kim, S.P.; Liu, L. Gravitational and electromagnetic radiation from binary black holes with electric and magnetic charges: Hyperbolic orbits on a cone. *Commun. Theor. Phys.* **2023**, *75*, 065401. [CrossRef]
121. Meng, D.S.; Yuan, C.; Huang, Q.G. Primordial black holes generated by the non-minimal spectator field. *Sci. China Phys. Mech. Astron.* **2023**, *66*, 280411. [CrossRef]

122. Garcia-Saenz, S.; Lu, Y.; Shuai, Z. Scalar-induced gravitational waves from ghost inflation and parity violation. *Phys. Rev. D* **2023**, *108*, 123507. [CrossRef]
123. Huang, Q.G.; Yuan, C.; Chen, Z.C.; Liu, L. GW230529_181500: A Potential Primordial Binary Black Hole Merger in the Mass Gap. *arXiv* **2024**, arXiv:2404.05691.
124. Chen, Z.C.; Hall, A. Confronting primordial black holes with LIGO-Virgo-KAGRA and the Einstein Telescope. *arXiv* **2024**, arXiv:2402.03934.
125. Martin, J.; Motohashi, H.; Suyama, T. Ultra Slow-Roll Inflation and the non-Gaussianity Consistency Relation. *Phys. Rev. D* **2013**, *87*, 023514. [CrossRef]
126. Motohashi, H.; Starobinsky, A.A.; Yokoyama, J. Inflation with a constant rate of roll. *JCAP* **2015**, *09*, 018. [CrossRef]
127. Yi, Z.; Gong, Y. On the constant-roll inflation. *JCAP* **2018**, *03*, 052. [CrossRef]
128. Yi, Z.; Gong, Y. Nonminimal coupling and inflationary attractors. *Phys. Rev. D* **2016**, *94*, 103527. [CrossRef]
129. Fei, Q.; Gong, Y.; Lin, J.; Yi, Z. The reconstruction of tachyon inflationary potentials. *JCAP* **2017**, *08*, 018. [CrossRef]
130. Garcia-Bellido, J.; Ruiz Morales, E. Primordial black holes from single field models of inflation. *Phys. Dark Univ.* **2017**, *18*, 47–54. [CrossRef]
131. Germani, C.; Prokopec, T. On primordial black holes from an inflection point. *Phys. Dark Univ.* **2017**, *18*, 6–10. [CrossRef]
132. Motohashi, H.; Hu, W. Primordial Black Holes and Slow-Roll Violation. *Phys. Rev. D* **2017**, *96*, 063503. [CrossRef]
133. Ezquiaga, J.M.; Garcia-Bellido, J.; Ruiz Morales, E. Primordial Black Hole production in Critical Higgs Inflation. *Phys. Lett. B* **2018**, *776*, 345–349. [CrossRef]
134. Yi, Z.; Gong, Y. Gauss–Bonnet Inflation and the String Swampland. *Universe* **2019**, *5*, 200. [CrossRef]
135. Yi, Z.; Gong, Y.; Sabir, M. Inflation with Gauss–Bonnet coupling. *Phys. Rev. D* **2018**, *98*, 083521. [CrossRef]
136. Ballesteros, G.; Beltran Jimenez, J.; Pieroni, M. Black hole formation from a general quadratic action for inflationary primordial fluctuations. *JCAP* **2019**, *06*, 016. [CrossRef]
137. Dalianis, I.; Kehagias, A.; Tringas, G. Primordial black holes from α-attractors. *JCAP* **2019**, *01*, 037. [CrossRef]
138. Bezrukov, F.; Pauly, M.; Rubio, J. On the robustness of the primordial power spectrum in renormalized Higgs inflation. *JCAP* **2018**, *02*, 040. [CrossRef]
139. Kannike, K.; Marzola, L.; Raidal, M.; Veermäe, H. Single Field Double Inflation and Primordial Black Holes. *JCAP* **2017**, *09*, 020. [CrossRef]
140. Fei, Q.; Yi, Z.; Yang, Y. The Reconstruction of Non-Minimal Derivative Coupling Inflationary Potentials. *Universe* **2020**, *6*, 213. [CrossRef]
141. Lin, J.; Gao, Q.; Gong, Y.; Lu, Y.; Zhang, C.; Zhang, F. Primordial black holes and secondary gravitational waves from k and G inflation. *Phys. Rev. D* **2020**, *101*, 103515. [CrossRef]
142. Lin, J.; Gao, S.; Gong, Y.; Lu, Y.; Wang, Z.; Zhang, F. Primordial black holes and scalar induced gravitational waves from Higgs inflation with noncanonical kinetic term. *Phys. Rev. D* **2023**, *107*, 043517. [CrossRef]
143. Yi, Z.; Zhu, Z.H. Inflationary attractors from a non-canonical kinetic term. *arXiv* **2021**, arXiv:2106.10303.
144. Gao, Q.; Gong, Y.; Yi, Z. Primordial black holes and secondary gravitational waves from natural inflation. *Nucl. Phys. B* **2021**, *969*, 115480. [CrossRef]
145. Gao, Q.; Gong, Y.; Yi, Z. On the constant-roll inflation with large and small η_H. *Universe* **2019**, *5*, 215. [CrossRef]
146. Gao, Q. Primordial black holes and secondary gravitational waves from chaotic inflation. *Sci. China Phys. Mech. Astron.* **2021**, *64*, 280411. [CrossRef]
147. Yi, Z.; Gong, Y.; Wang, B.; Zhu, Z.h. Primordial black holes and secondary gravitational waves from the Higgs field. *Phys. Rev. D* **2021**, *103*, 063535. [CrossRef]
148. Yi, Z.; Gao, Q.; Gong, Y.; Zhu, Z.h. Primordial black holes and scalar-induced secondary gravitational waves from inflationary models with a noncanonical kinetic term. *Phys. Rev. D* **2021**, *103*, 063534. [CrossRef]
149. Yi, Z.; Zhu, Z.H. NANOGrav signal and LIGO-Virgo primordial black holes from the Higgs field. *JCAP* **2022**, *05*, 046. [CrossRef]
150. Yi, Z. Primordial black holes and scalar-induced gravitational waves from the generalized Brans-Dicke theory. *JCAP* **2023**, *03*, 048. [CrossRef]
151. Zhang, F.; Gong, Y.; Lin, J.; Lu, Y.; Yi, Z. Primordial non-Gaussianity from G-inflation. *JCAP* **2021**, *04*, 045. [CrossRef]
152. Pi, S.; Zhang, Y.l.; Huang, Q.G.; Sasaki, M. Scalaron from R^2-gravity as a heavy field. *JCAP* **2018**, *05*, 042. [CrossRef]
153. Kamenshchik, A.Y.; Tronconi, A.; Vardanyan, T.; Venturi, G. Non-Canonical Inflation and Primordial Black Holes Production. *Phys. Lett. B* **2019**, *791*, 201–205. [CrossRef]
154. Fu, C.; Wu, P.; Yu, H. Primordial Black Holes from Inflation with Nonminimal Derivative Coupling. *Phys. Rev. D* **2019**, *100*, 063532. [CrossRef]
155. Fu, C.; Wu, P.; Yu, H. Scalar induced gravitational waves in inflation with gravitationally enhanced friction. *Phys. Rev. D* **2020**, *101*, 023529. [CrossRef]
156. Dalianis, I.; Karydas, S.; Papantonopoulos, E. Generalized Non-Minimal Derivative Coupling: Application to Inflation and Primordial Black Hole Production. *JCAP* **2020**, *06*, 040. [CrossRef]
157. Gundhi, A.; Steinwachs, C.F. Scalaron–Higgs inflation reloaded: Higgs-dependent scalaron mass and primordial black hole dark matter. *Eur. Phys. J. C* **2021**, *81*, 460. [CrossRef]

158. Cheong, D.Y.; Lee, S.M.; Park, S.C. Primordial black holes in Higgs-R^2 inflation as the whole of dark matter. *JCAP* **2021**, *01*, 032. [CrossRef]
159. Zhang, F. Primordial black holes and scalar induced gravitational waves from the E model with a Gauss–Bonnet term. *Phys. Rev. D* **2022**, *105*, 063539. [CrossRef]
160. Zhang, F.; Lin, J.; Lu, Y. Double-peaked inflation model: Scalar induced gravitational waves and primordial-black-hole suppression from primordial non-Gaussianity. *Phys. Rev. D* **2021**, *104*, 063515. Erratum in *Phys. Rev. D* **2021**, *104*, 129902. [CrossRef]
161. Kawai, S.; Kim, J. Primordial black holes from Gauss–Bonnet-corrected single field inflation. *Phys. Rev. D* **2021**, *104*, 083545. [CrossRef]
162. Cai, R.G.; Chen, C.; Fu, C. Primordial black holes and stochastic gravitational wave background from inflation with a noncanonical spectator field. *Phys. Rev. D* **2021**, *104*, 083537. [CrossRef]
163. Chen, P.; Koh, S.; Tumurtushaa, G. Primordial black holes and induced gravitational waves from inflation in the Horndeski theory of gravity. *arXiv* **2021**, arXiv:2107.08638.
164. Karam, A.; Koivunen, N.; Tomberg, E.; Vaskonen, V.; Veermäe, H. Anatomy of single-field inflationary models for primordial black holes. *JCAP* **2023**, *03*, 013. [CrossRef]
165. Ashoorioon, A.; Rostami, A.; Firouzjaee, J.T. EFT compatible PBHs: Effective spawning of the seeds for primordial black holes during inflation. *JHEP* **2021**, *07*, 087. [CrossRef]
166. Liu, J.; Gong, Y.; Yi, Z. Constant-roll inflation with non-minimally derivative coupling. *arXiv* **2024**, arXiv:2404.04978.
167. Dandoy, V.; Domcke, V.; Rompineve, F. Search for scalar induced gravitational waves in the international pulsar timing array data release 2 and NANOgrav 12.5 years datasets. *SciPost Phys. Core* **2023**, *6*, 060. [CrossRef]
168. Linde, A.D. A New Inflationary Universe Scenario: A Possible Solution of the Horizon, Flatness, Homogeneity, Isotropy and Primordial Monopole Problems. *Phys. Lett. B* **1982**, *108*, 389–393. [CrossRef]
169. Albrecht, A.; Steinhardt, P.J. Cosmology for Grand Unified Theories with Radiatively Induced Symmetry Breaking. *Phys. Rev. Lett.* **1982**, *48*, 1220–1223. [CrossRef]
170. Harigaya, K.; Inomata, K.; Terada, T. Induced gravitational waves with kination era for recent pulsar timing array signals. *Phys. Rev. D* **2023**, *108*, 123538. [CrossRef]
171. Kawasaki, M.; Kohri, K.; Sugiyama, N. Cosmological constraints on late time entropy production. *Phys. Rev. Lett.* **1999**, *82*, 4168. [CrossRef]
172. Kawasaki, M.; Kohri, K.; Sugiyama, N. MeV scale reheating temperature and thermalization of neutrino background. *Phys. Rev. D* **2000**, *62*, 023506. [CrossRef]
173. Hannestad, S. What is the lowest possible reheating temperature? *Phys. Rev. D* **2004**, *70*, 043506. [CrossRef]
174. Hasegawa, T.; Hiroshima, N.; Kohri, K.; Hansen, R.S.L.; Tram, T.; Hannestad, S. MeV-scale reheating temperature and thermalization of oscillating neutrinos by radiative and hadronic decays of massive particles. *JCAP* **2019**, *12*, 012. [CrossRef]
175. Ashton, G.; Hübner, M.; Lasky, P.D.; Talbot, C.; Ackley, K.; Biscoveanu, S.; Chu, Q.; Divakarla, A.; Easter, P.J.; Goncharov, B.; et al. BILBY: A user-friendly Bayesian inference library for gravitational-wave astronomy. *Astrophys. J. Suppl.* **2019**, *241*, 27. [CrossRef]
176. Skilling, J. Nested Sampling. *AIP Conf. Proc.* **2004**, *735*, 395–405. [CrossRef]
177. Moore, C.J.; Vecchio, A. Ultra-low-frequency gravitational waves from cosmological and astrophysical processes. *Nat. Astron.* **2021**, *5*, 1268–1274. [CrossRef]
178. Lamb, W.G.; Taylor, S.R.; van Haasteren, R. Rapid refitting techniques for Bayesian spectral characterization of the gravitational wave background using pulsar timing arrays. *Phys. Rev. D* **2023**, *108*, 103019. [CrossRef]
179. Johnson, M.C.; Kamionkowski, M. Dynamical and Gravitational Instability of Oscillating-Field Dark Energy and Dark Matter. *Phys. Rev. D* **2008**, *78*, 063010. [CrossRef]
180. Turner, M.S. Coherent Scalar Field Oscillations in an Expanding Universe. *Phys. Rev. D* **1983**, *28*, 1243. [CrossRef]
181. Armendariz-Picon, C.; Mukhanov, V.F.; Steinhardt, P.J. Essentials of k essence. *Phys. Rev. D* **2001**, *63*, 103510. [CrossRef]
182. Silverstein, E.; Tong, D. Scalar speed limits and cosmology: Acceleration from D-cceleration. *Phys. Rev. D* **2004**, *70*, 103505. [CrossRef]
183. Liddle, A.R.; Leach, S.M. How long before the end of inflation were observable perturbations produced? *Phys. Rev. D* **2003**, *68*, 103503. [CrossRef]
184. Allahverdi, R.; Brandenberger, R.; Cyr-Racine, F.Y.; Mazumdar, A. Reheating in Inflationary Cosmology: Theory and Applications. *Ann. Rev. Nucl. Part. Sci.* **2010**, *60*, 27–51. [CrossRef]
185. Kofman, L.; Linde, A.D.; Starobinsky, A.A. Reheating after inflation. *Phys. Rev. Lett.* **1994**, *73*, 3195–3198. [CrossRef] [PubMed]
186. Kofman, L.; Linde, A.D.; Starobinsky, A.A. Towards the theory of reheating after inflation. *Phys. Rev. D* **1997**, *56*, 3258–3295. [CrossRef]
187. Domènech, G. Induced gravitational waves in a general cosmological background. *Int. J. Mod. Phys. D* **2020**, *29*, 2050028. [CrossRef]
188. Dufaux, J.F.; Bergman, A.; Felder, G.N.; Kofman, L.; Uzan, J.P. Theory and Numerics of Gravitational Waves from Preheating after Inflation. *Phys. Rev. D* **2007**, *76*, 123517. [CrossRef]

Disclaimer/Publisher's Note: The statements, opinions and data contained in all publications are solely those of the individual author(s) and contributor(s) and not of MDPI and/or the editor(s). MDPI and/or the editor(s) disclaim responsibility for any injury to people or property resulting from any ideas, methods, instructions or products referred to in the content.